JOURNAL OF CATALYSIS 121, 236–247 (1990)

Surface Organometallic Chemistry on Metals

III. Formation of a Bimetallic Ni–Sn Phase Generated by Reaction of a $Sn(n\text{-}C_4H_9)_4$ and Silica-Supported Nickel Oxide

M. AGNELLI,*,[1] J. P. CANDY,* J. M. BASSET,* J. P. BOURNONVILLE,† AND O. A. FERRETTI†

*Institut de Recherches sur la Catalyse, Laboratoire Propre du CNRS, conventionné à l'Université Claude Bernard, Lyon 1, 2 Avenue Albert Einstein, 69626 Villeurbanne Cédex, France, and †Institut Français du Pétrole, 2-4 Av. de Bois-Préau, 92506 Rueil-Malmaison Cédex, France

Received December 22, 1988; revised May 15, 1989

Reaction of $Sn(n\text{-}C_4H_9)_4$ with NiO/SiO_2 occurs above 423 K according to the apparent following stoichiometry: $NiO + xSn(n\text{-}C_4H_9)_4 \rightarrow NiSn_x + (2x + 1)C_4H_8 + (2x - 1)C_4H_{10} + H_2O$. Various compositions of the bimetallic phase can be achieved by changing the initial Sn/Ni ratio. The obtained catalysts were very active and selective in the hydrogenation of ethyl acetate to ethanol. Characterization of the bimetallic phase has shown that the particles are bimetallic (STEM). As a result of chemisorption, IR, and magnetic measurements, it appears that the presence of tin has four effects: (i) it decreases significantly the amount of CO and H_2 adsorbed; (ii) it isolates nickel atoms from their neighbors; (iii) it increases electron density on nickel; and (iv) it suppresses the magnetic properties of nickel. Redox behavior of $Ni–Sn/SiO_2$ toward surface OH indicates that surface hydroxyls can oxidize $Sn^{(0)}$, probably to $Sn^{(II)}$ with evolution of H_2, the process being reversible with H_2. It is suggested that during this oxidation process, tin migrates to the periphery of the bimetallic particle with formation of $(\geqslant Si–O)_2Sn^{(II)}$ surface species.

1. INTRODUCTION

The preparation of new catalytic materials which exhibit increased stereo-, regio-, and chemoselectivity in catalytic reactions involving polyfunctional organic molecules has attracted great interest in the last decades. Regarding this aspect of catalysis, there are indications in the literature that the association of two metals may lead to more selective and (or) more active catalysts. For example, significant changes in the catalytic properties of Group VIII transition metals (e.g., Rh, Ni, Pd, Pt) have been observed by alloy formation with other metals (e.g., Sn, Sb) (*1*, *2*).

Surface organometallic chemistry provides an excellent tool for preparing bimetallic catalysts based on metals of Groups VIII and IV. For example, Travers *et al.* (*3*) have demonstrated that the reaction of $Sn(n\text{-}C_4H_9)_4$ with Rh supported on alumina or silica resulted in a new catalytic material which is more active and more selective than supported Rh with respect to the hydrogenation of ethyl acetate to ethanol. Recently, similar catalytic results have been obtained with silica supported Ni–Sn catalysts obtained by reaction between Ni/SiO_2 and $Sn(n\text{-}C_4H_9)_4$ (*4*, *5*).

An understanding of the chemistry of the preparation of these bimetallic catalysts is just in its beginnings (*5*). The aim of this work is to describe the chemistry of the reaction between Ni/SiO_2 and $Sn(n\text{-}C_4H_9)_4$ to characterize the bimetallic $Ni–Sn/SiO_2$ catalysts, and to evaluate their catalytic activity and selectivity toward the hydrogenation of ethyl acetate to ethanol.

[1] On leave from Centro de Investigation y Desarollo en Processus Cataliticos, 47 No. 257, (1900) La Plata, Argentina.

0021-9517/90 $3.00

2. EXPERIMENTAL

2.1. Preparation of NiO/SiO_2

Silica (Aerosil from Degussa) used as a support exhibited a surface area of 200 m^2 g^{-1}. It was used as such without any special pretreatment. NiO supported on this silica was prepared by an ion-exchange method from $[Ni(NH_3)_6]^{2+}$ (*6*). The surface protons of the starting silica were first exchanged with ammonium by stirring 10 g of silica with 50 ml of ammonia (pH 10.2) for 30 min. Then the solid was filtered off and contacted with a solution of $[Ni(NH_3)_6]^{2+}$. The following exchange reaction occurred:

$$2\geqslant Si{-}O{-}NH_4 + [Ni(NH_3)_6]^{2+} \rightarrow [\geqslant Si{-}O]_2^- [Ni(NH_3)_6]^{2+} + 2NH_4^+.$$

The slurry was continuously agitated for 24 h and then filtered. After this, the nickel complex adsorbed on the surface was decomposed with loss of NH_3 at 353 K *in vacuo* and, as a result, a $Ni(OH)_2$ species was formed on the surface. The supported $Ni(OH)_2$ was then decomposed in a hydrogen stream (1.033 bar) (1 bar = 10^5 N m^{-2}) at 723 K following the temperature schedule suggested by Bartholomew and Farranto (*7*) to favor heat and mass transfer. Once reduced, the catalyst was passivated at room temperature in a flow of nitrogen containing 1% of oxygen. This procedure was carried out in order to avoid particle sintering (*7*). (When the catalyst is directly exposed to air, since the enthalphy of Ni oxidation at room temperature is large and negative ($\Delta H = -58.4$ kcal/mol for NiO), a large increase in temperature leading to sintering can be expected).

2.2 Techniques for Catalyst Characterization

Transmission electron microscopy (TEM). Particle size distribution was directly obtained from micrographs photographically enlarged, using a JEOL Jem 100 CX instrument. Each histogram was constructed from a statistical number of particles oscillating around 500.

Scanning transmission electron microscopy (STEM). Qualitative and quantitative chemical analyses of bimetallic particles were performed by means of a Vacuum Generator HB 501 scanning transmission microscope with a Si-Li detector connected to a multichannel analyzer. This dedicated STEM is equipped with a field-emission gun giving a high current density electron beam. After demagnification by the objective lens, the electron probe is as small as 0.5 nm on the specimen. The spatial resolution of analysis is such that 1 nm^2 of projected area of the sample can be analyzed selectivity. Tin was acquired on the $L\alpha$ band (3.44 keV) and Ni on the $K\alpha$ band (7.47 keV).

Magnetic measurements. Magnetic measurements can give information on the morphology of reduced catalysts (degree of reduction, metallic particle size) and on the modifications induced by the introduction of a promoter to a pure ferromagnetic metal (*8*).

The magnetization of the thoroughly reduced and evacuated samples was measured in an electromagnet (fields up to 21 k0e) at room temperature using the Weiss extraction method (*8*). The system was calibrated using unsupported pure nickel. The degree of reduction was calculated from saturation data and two metallic particle sizes were evaluated from magnetization data at high and low magnetic fields (D_1 and D_2, respectively). The average diameter of surface D_s may be deduced from those values by the simple equation (*9*)

$$D_s = (D_1 + D_2)/2.$$

Dispersion of nickel particles can also be deduced from magnetic measurements carried out in the presence and in the absence of H_2 (*8*). If one assumes that each chemisorbed hydrogen atom cancels the magnetization of one surface nickel atom, one can deduce the dispersion from the magnetization of the sample before ($M_1 = K \cdot Ni_{total}$) and after ($M_2 = K \cdot Ni_{bulk}$) hydrogen chemi-

sorption: $\% D = Ni_{surface}/Ni_{total} = (M_1 - M_2)/M_1$.

Hydrogen and carbon monoxide chemisorption measurements. Gas adsorption measurements were carried out at room temperature in a conventional Pyrex volumetric adsorption apparatus, which was evacuated by means of mercury diffusion and rotary pumps (10^{-6} mbar) isolated from the adsorption system by a liquid-nitrogen-cooled trap. The catalyst sample was placed in a Pyrex flow-through cell to enable reduction in flowing hydrogen at 723 K before the chemisorption measurements. After reduction, the sample was outgassed at 573 K for 1 h under vacuum. The amount of gas adsorbed by the catalyst was determined from the gas pressure drop measured with a Texas Instruments pressure gauge.

Metal dispersion (% *D*) was calculated from H_2 uptake assuming a stoichiometry of one hydrogen atom per nickel surface atom. Average crystallite diameter (D_s) was evaluated using the equation

$$D_s = 971/\% D$$

based on the assumption that all the crystallites are spherical and of the same size (*10*).

Infrared spectroscopy. Infrared spectra of CO adsorbed on the reduced catalyst were taken with an IR-FT Nicolet 10 MX spectrometer. Catalyst samples were compressed under a pressure of 2 T/cm^2 and introduced into a Pyrex cell which permitted the same pretreatment as that described for volumetric adsorption. Then, CO was admitted into the cell and evacuated after 30 min by pumping (this procedure avoids detection of the $Ni(CO)_4$ eventually formed or prevents its formation to a significant extent). The spectrum of chemisorbed CO was directly computed by subtraction of the Ni/SiO_2 background.

Reaction between $Sn(n\text{-}C_4H_9)_4$ and NiO/SiO_2. The interaction between $Sn(n\text{-}C_4H_9)_4$ and NiO/SiO_2 has been studied as a function of temperature by measuring the amount of gas evolved when $Sn(n\text{-}C_4H_9)_4$ was allowed to react with supported NiO. For this purpose, a sample of the passivated catalyst was introduced into the reactor. Then, a given amount of tetra-*n*-butyltin was admitted. Temperature was raised stepwise (50-K increments) by means of an electric furnace and maintained for 1 h before the next increment. At every step, the products of reaction were collected in a liquid nitrogen trap. After heating to room temperature, the pressure in the system was measured to obtain the total amount of evolved gases. The products were analyzed by gas chromatography.

2.3. Ethyl Acetate Hydrogenation

The hydrogenation of ethyl acetate was carried out in a conventional fixed-bed flow differential reactor at 523 K under 4.5 MPa of H_2 and 0.5 MPa of ethyl acetate. The contact time was varied between 4 and 40 (wwh). Activity was defined as the number of moles of ethyl acetate transformed per gram of catalyst per hour, whereas selectivity (S_i) was defined as the ratio of the carbon weight in product (*i*) against the total carbon weight in all the products.

Prior to catalytic measurements, the samples were treated *in situ* in flowing hydrogen (5 MPa, 8 mol $H_2/h \cdot g$) at 373 K (1 h), 523 K (1 h), and 723 K (2 h). Then the temperature was adjusted to the reaction temperature and the reactive reagents were introduced at the desired rates. After 2 h the products were analyzed by the gas chromatographic technique.

For $Ni–Sn/SiO_2$ catalysts, the measured catalytic activity and selectivity did not vary with time on stream as the values measured after 24 h were equal to the initial values (2 h) (within the experimental error: ±2%).

3. RESULTS AND DISCUSSION

3.1. Preparation and Characterization of Mono- and Bimetallic Catalysts

3.1.a. Characterization of Ni/SiO_2. A histogram of particle size distribution of Ni/SiO_2 (3% wt) is shown in Fig. 1a. The distri-

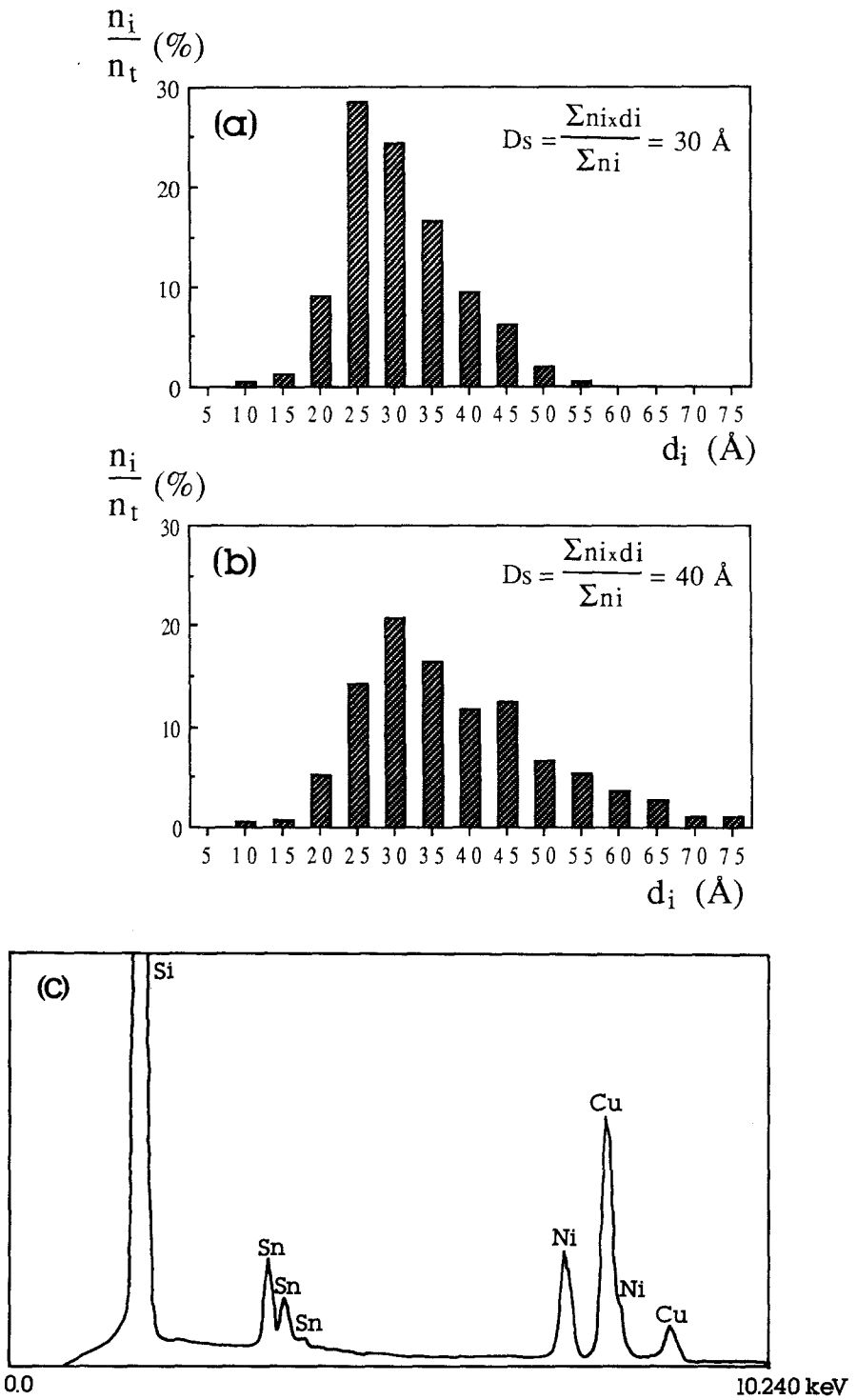

FIG. 1. Histogram of particle size distribution of: (a) silica-supported Ni catalyst; (b) silica-supported Ni–Sn catalyst (Sn/Ni = 1.7); (c) scanning transmission electron microscope analysis of Ni–Sn catalyst (Sn/Ni = 1.7).

TABLE 1

Characteristics of Ni/SiO_2 Evaluated by Magnetic TEM Measurements and Hydrogen Adsorption

Characteristic	Technique		
	Magnetic measurements	H_2 adsorption	TEM
Degree of red	58%		
D_1	34 Å		
D_2	40 Å		
D_s	37 Å	30 Å	30 Å
% D	31%	32%	
H_2 uptake		81.5 μml/g	

bution is rather narrow with an average diameter D_s of 30 Å. (1 Å = 0.1 nm). This value is in fairly good agreement with those deduced from magnetic measurements (37 Å) or H_2 chemisorption data (30 Å) (Table 1). One should note (Table 1) that only 58% of Ni is reduced according to ferromagnetic data.

For Ni/SiO_2, H_2 and CO adsorption isotherms at 298 K are given in Figs. 2a and 3a, respectively. The isotherm of CO adsorption is not very reliable because, for each partial pressure of CO, a continuous and slow consumption occurs, corresponding to the well-known process of $Ni(CO)_4$ formation. This phenomenon has been checked independently by infrared spectroscopy. In contrast, H_2 uptake is fast and leads to a plateau for a hydrogen pressure higher than ca. 100 mbar.

CO is irreversibly adsorbed at room temperature on Ni/SiO_2 and gives rise to two infrared absorption bands at 2077 and 1933 cm^{-1} corresponding to linear and bridged coordinated CO (*9*) (Fig. 4a).

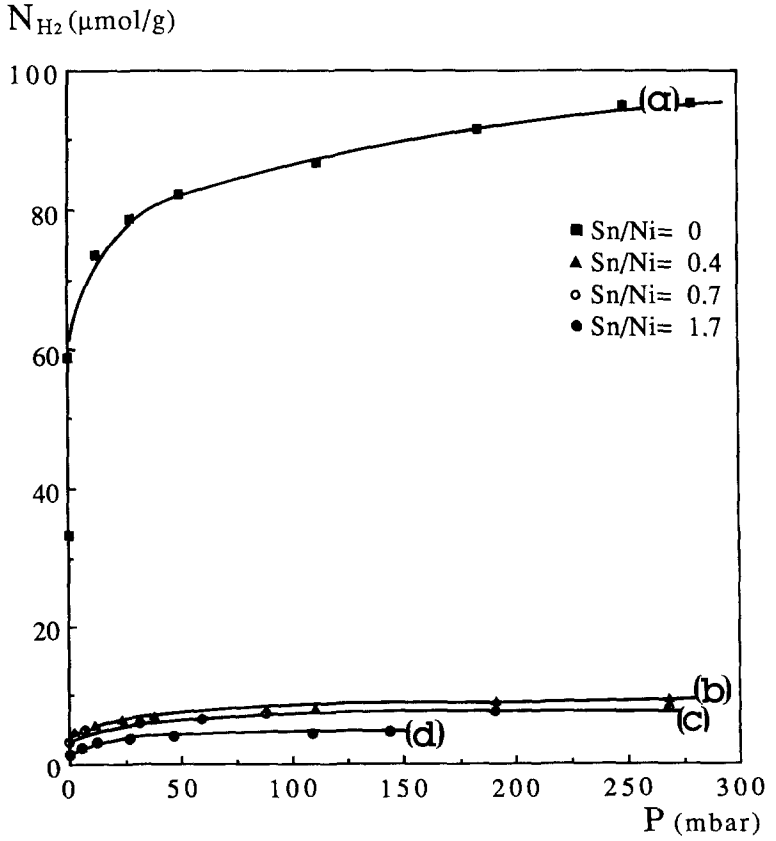

FIG. 2. Hydrogen adsorption isotherms at room temperature on: (a) Ni/SiO_2; and (b, c, and d) Ni–Sn/SiO_2.

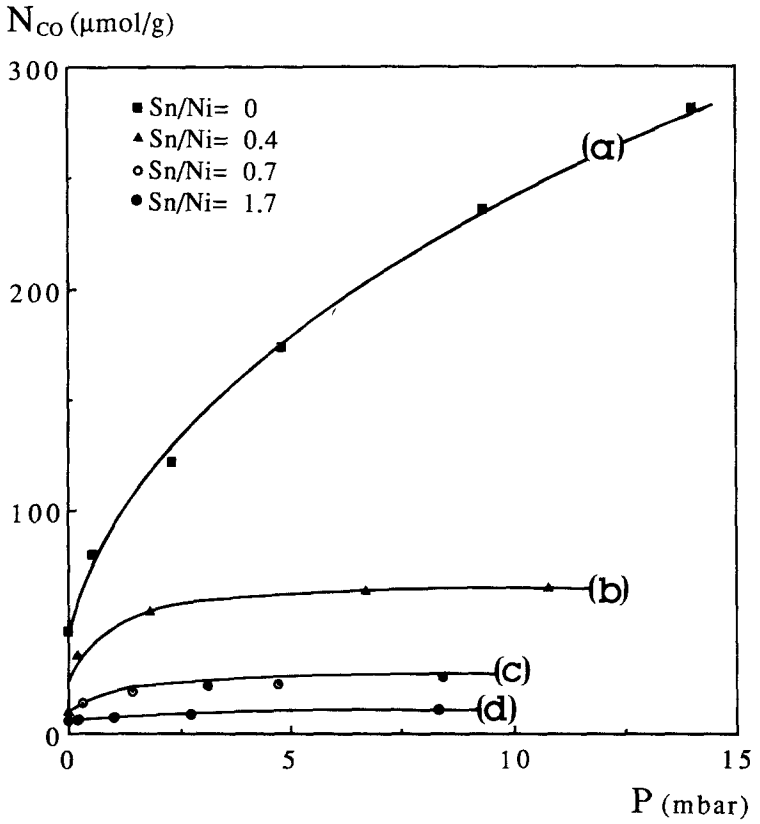

FIG. 3. Carbon monoxide adsorption isotherms at room temperature on: (a) Ni/SiO_2; and (b, c, and d) $Ni–Sn/SiO_2$.

3.1.b.1. Preliminary results on the reaction of $Sn(n\text{-}C_4H_9)_4$ with NiO/SiO_2. As mentioned under Experimental, interaction between $Sn(n\text{-}C_4H_9)_4$ with SiO_2 or NiO/SiO_2 was first studied in the absence of any solvent as a function of temperature. The reaction was followed by analyzing the gases given off at a given temperature.

Reaction of pure $Sn(n\text{-}C_4H_9)_4$ (1.51 m·mol) with a silica (0.665 g) previously dehydroxylated at 473 K ($SiO_2(473)$) gives rise to the evolution of small amounts of *n*-butane even at 573 K (Fig. 5a).

Reaction of $Sn(n\text{-}C_4H_9)_4$ (1.2 mmol) with NiO/SiO_2 (473) (0.5043 g) starts at ca. 320 K. It gives rise to the evolution of much larger amounts of *n*-butane and *n*-butenes than those observed on pure silica. The total amount of butane and *n*-butenes evolved at 600 K corresponds to the transformation of all the butyl groups of $Sn(n\text{-}C_4H_9)_4$.

A detailed analysis of the product distribution for each increment of temperature (Fig. 5b) indicates that the ratio *n*-butenes/*n*-butane is always higher than unity, suggesting a progressive reduction of Ni^{+2} to $Ni^{(0)}$. Moreover, among *n*-butenes, 1-butene, which is the thermodynamically unfavored isomer, is always the major one, especially above 473 K. The selective formation of 1-butene suggests a transfer of a β-H atom either from one butyl group to a second butyl group to form butane, or from one butyl group to nickel oxide to reduce it.

Apparently, the overall surface reaction obeys a general stoichiometric equation

$$NiO + xSn(n\text{-}C_4H_9)_4 \rightarrow NiSn_x + H_2O + (2x + 1)C_4H_8 + (2x - 1)C_4H_{10}.$$

For example when the Sn/Ni ratio was equal to 4, the overall ratio *n*-butenes/*n*-

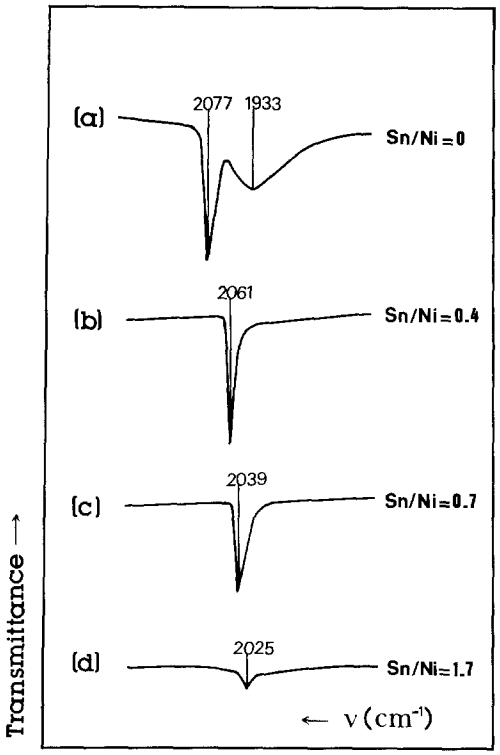

FIG. 4. Infrared spectroscopy of CO irreversibly adsorbed at room temperature on: (a) Ni/SiO_2; and (b, c, and d) $Ni–Sn/SiO_2$.

butane was found to be equal to 9.2/6.8 which is very close to the value (9/7) corresponding to the simple equation

$$NiO + 4Sn(n\text{-}C_4H_9)_4 \rightarrow NiSn_4 + 9C_4H_8 + 7C_4H_{10} + H_2O.$$

3.1.b.2. Preparation of $NiSn/SiO_2$ catalysts via a solvent. As we have stated above, tetra-*n*-butyl-tin reacts with NiO/SiO_2 only at temperatures greater than 423 K. For that reason, *n*-dodecane, for which the boiling point is 444 K, was chosen as a solvent for the preparation of the bimetallic catalyst. The following procedure was used: $Sn(n\text{-}C_4H_9)_4$ and NiO/SiO_2 were heated under a stream of Ar up to the dodecane reflux temperature and kept at this temperature for 48 h. Then, the resulting solid was filtered, washed with *n*-heptane, and dried in flowing Ar.

Experimental conditions as well as analytical data are listed in Table 2. As can be clearly seen, the quantity of tin fixed is always smaller than the amount of tin that was initially introduced.

3.1.c. Characterization of the bimetallic $Ni–Sn/SiO_2$ catalysts. A particle size distribution histogram of $Ni–Sn/SiO_2$ (Sn/Ni = 1.7) is shown in Fig. 1b. The average diameter D_s is, in this case, 40 Å and the distribution broadens toward diameters greater than that observed for Ni/SiO_2. Scanning transmission electron microscope analysis always shows the peak of Sn (3.44 keV) associated with that of Ni (4.47 keV) (Fig. 1c). The atomic Sn/Ni ratio determined by STEM analysis (Sn/Ni = 1.4) is rather close to the value obtained by chemical analysis (Sn/Ni = 1.7). Particles of Sn were never found alone on the support.

Magnetic measurements on $Ni–Sn/SiO_2$ indicated that samples with a ratio Sn/Ni = 0.4 had lost their ferromagnetic properties at room temperature. The saturation magnetization dropped to zero whereas for Ni/SiO_2 (3%) the value was as high as 31.8 CGS e.u. This result is in agreement with

TABLE 2

Experimental Conditions for the Preparation of Bimetallic Catalysts; Analytical Data Obtained after Reaction of $Sn(n\text{-}C_4H_9)_4$ with NiO/SiO_2 (in Refluxing Dodecane)

Catalyst No.	Catalyst mass (g)	Vol. of $Sn(n\text{-}C_4H_9)_4$ (μl)	% Sn introduced	% Sn found	(Sn/Ni) found
02	1.0506	500	14.6	9.4	1.7
05	2.1195	500	7.8	3.7	0.7
07	2.028	250	4.2	2.4	0.4

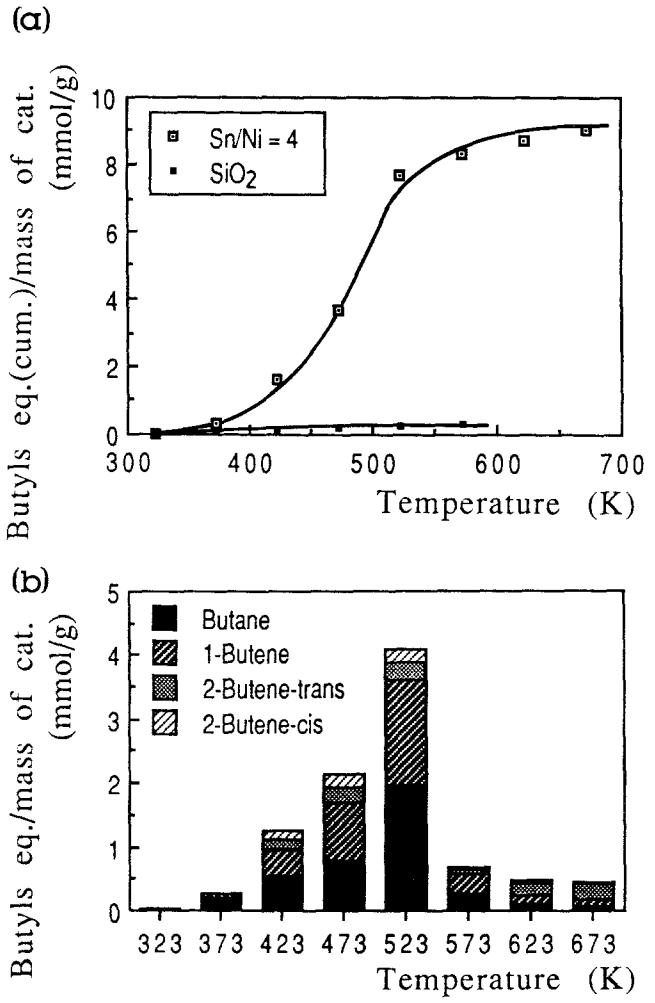

FIG. 5. (a) Cumulative amounts of butyl equivalents given off during $Sn(n\text{-}C_4H_9)_4$–NiO/SiO_2 and $Sn(n\text{-}C_4H_9)_4$–SiO_2 reactions (μmol/g) against temperature. (b) Amounts of butane and butenes given off at each temperature during $Sn(n\text{-}C_4H_9)_4$–NiO/SiO_2 reaction.

what is known for magnetic properties of alloys (*11*).

Isotherms of hydrogen adsorption for different tin contents are shown in Fig. 2b, 2c, and 2d). Hydrogen uptake diminishes abruptly compared to that observed for Ni/SiO_2 (Fig. 2a). Interestingly one should mention that it is not necessary to reach high Sn/Ni ratios to drastically suppress hydrogen uptake. Above a Sn/Ni ratio of 0.4, the decay of hydrogen uptake is negligible. This phenomenon has already been observed with alloys (*12–14*).

CO adsorption isotherms are shown in Fig. 3b, 3c, and 3d). In contrast to the case of hydrogen, CO uptake decreases progressively as the Sn/Ni ratio increases. Another important aspect can be drawn from this figure: the adsorption isotherms reach a "plateau," suggesting that there is no formation of $Ni(CO)_4$ in contrast to the case of Ni/SiO_2. This phenomenon has also been checked by infrared spectroscopy (before outgassing the sample).

Infrared spectra of CO irreversibly adsorbed on the bimetallic catalysts are

shown in Fig. 4b, 4c, and 4d) for different Sn/Ni ratios. Two important results deserve to be mentioned. First, only one absorption due to CO was observed. It is in the range of frequencies which can be reasonably assigned to CO linearly bonded to nickel (it is well known that tin does not chemisorb CO). The intensity of this band diminishes as the Sn/Ni ratio becomes greater. Secondly, as the Sn/Ni ratio increases, the absorption band shifts toward lower frequencies. The first phenomenon can be interpreted by both an effect of "site isolation" (*15, 16*) and an effect of surface poisoning due to tin. The second phenomenon, may be ascribed to an electronic effect of tin on Ni or to a lower surface coverage of CO as the Sn/Ni ratio increases. Both hypotheses lead to the same result (*9, 17*) which renders discrimination between them impossible. Nevertheless, the band shift observed in this case is greater than that reported in the literature on Ni/SiO_2 catalysts where the shift was due only to the degree of coverage. Thus, it is reasonable to propose the existence of an electronic interaction.

3.2. Redox Behavior of the Ni–Sn/SiO_2 System

Temperature-programmed desorption of hydrogen adsorbed on the reduced bimetallic catalyst was performed by Ferretti *et al.* (*4*). The results obtained for different Sn/Ni ratios are shown in Fig. 6. According to these data, hydrogen is desorbed at low temperature, approximately 473 K for Ni/SiO_2 catalysts. Meanwhile, in the case of bimetallics, two peaks of desorption are observed: one at low temperatures (473–573 K) and another at high temperatures (773–873 K). The appearance of this high-temperature peak of desorption is rather surprising.

This peak, for which the intensity is tin dependent, has also been observed for $Sn/Rh/SiO_2$ prepared via the organometallic route (*5*). It has been attributed to a redox reaction between silanols groups (or eventually molecular water) of the support and

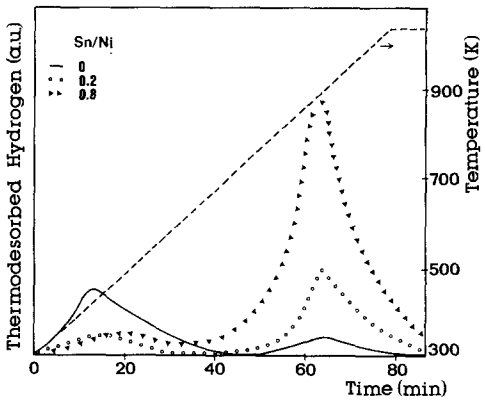

FIG. 6. Temperature-programmed desorption of adsorbed hydrogen on mono- and bimetallic catalysts in flowing Ar.

zerovalent tin:

$$x(\geqslant Si - OH) + Sn^{(0)} \rightarrow (\simeq Si\text{–}O)_x Sn^{x+} + \frac{x}{2} H_2$$

$$H_2O + Sn^{(0)} \rightarrow SnO + H_2$$

$$H_2O + Sn^{(0)} \rightarrow SnO_2 + 2\,H_2.$$

If this explanation is also valid for the Ni–Sn/SiO_2 system, after oxidation of tin by surface OH (or molecular water) tin should be present as $(\geqslant Si\text{–}O)_2Sn^{II}$, as $Sn^{II}O$, or as $Sn^{IV}O_2$. In any case, tin should have less interaction with nickel due to the disappearance of the alloy effect or to a migration of the zerovalent tin overlayer to the support or to both. Thus chemisorption properties should be quite different.

In order to check these hypotheses, chemisorption measurements of CO and H_2 were performed. Three bimetallic Ni–Sn/SiO_2 catalysts (Sn/Ni = 0.4, 0.7, 1.7) were reduced in flowing H_2 at 723 K and then evacuated (10^{-6} mbar) at 773 K for 2 h. After such treatment, the catalysts were cooled under vacuum to room temperature and then submitted to H_2 or CO pressure. Interestingly, their chemisorption properties toward H_2 were practically unchanged with respect to those of the same reduced bimetallic samples which had been evacuated at a temperature where Sn oxidation

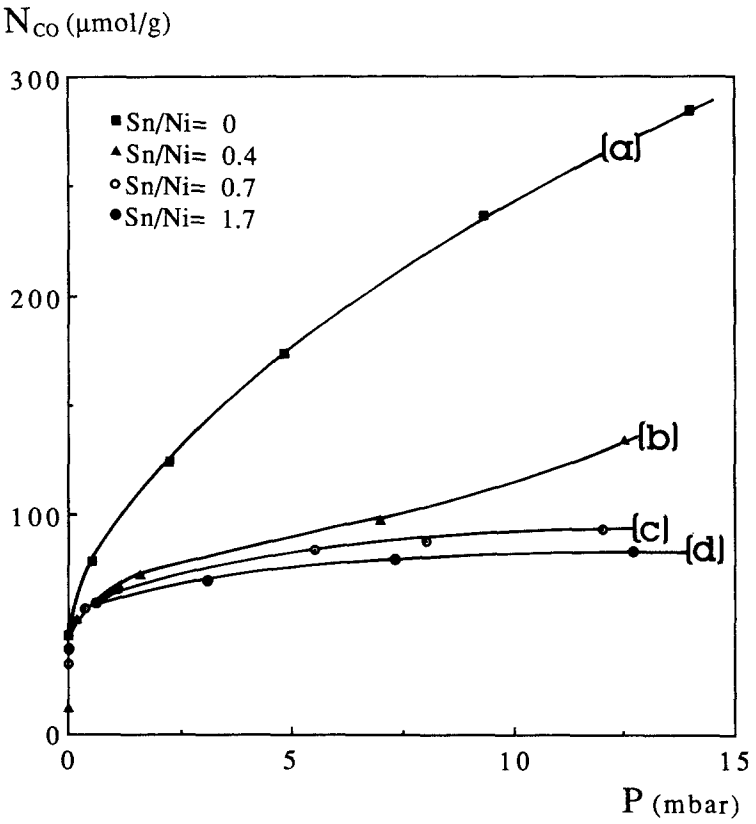

FIG. 7. Carbon monoxide adsorption isotherms of Ni–Sn/SiO_2 catalysts at room temperature after treatment *in vacuo* at 773 K.

does not occur (573 K) (Fig. 2b, 2c, and 2d). In contrast, CO adsorption on the bimetallic catalysts evacuated at higher temperature (773 K) exhibited a higher CO uptake than that obtained for the same catalyst evacuated at lower temperature (Fig. 7). The restoration of the chemisorption ability toward CO after high-temperature evacuation was also checked independently by infrared spectroscopy (Fig. 8). After high-temperature evacuation (773 K, 10^{-6} mbar), the intensity of the absorption band was restored and its frequency had shifted back to higher values. However, the band due to bridging CO was not restored. This result suggests that tin is, at least partially, present in the particle after high-temperature evacuation. This was independently checked by STEM experiments.

A subsequent treatment of a Sn/Ni = 1.7 sample under H_2 at 723 K for 16 h, followed by CO chemisorption at room temperature, restored the spectrum of Fig. 4d, indicating the complete reversibility of the redox phenomena.

Apparently, and to a first approximation, the bimetallic catalyst, after reduction under flowing hydrogen at 723 K for 16 h can be described as particles of Ni–Sn alloy. High-temperature (723 K) treatment *in vacuo* or in flowing Ar results in the specific oxidation of Sn by silanols groups of the support which can migrate to the periphery of the particles. Under these conditions, tin is "extracted" from the Ni–Sn alloy, leading to a decrease in the Sn/Ni ratio in the alloy.

3.3. Ethyl Acetate Hydrogenation

The introduction of tin to nickel via the organometallic route results in a new catalytic material which exhibits a very high se-

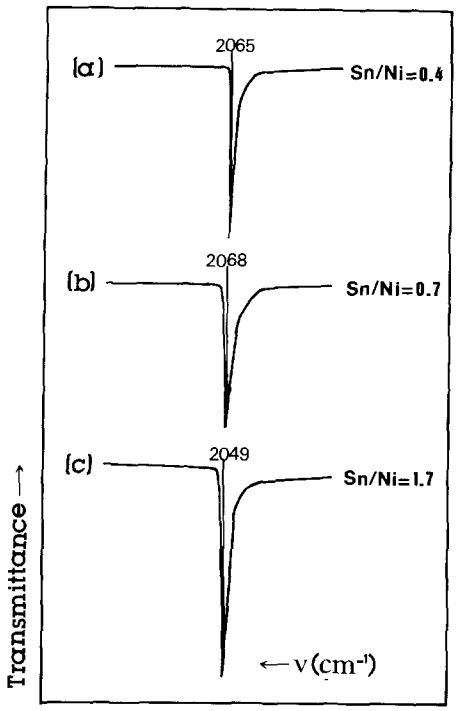

FIG. 8. Infrared spectroscopy of CO adsorbed on Ni–Sn/SiO_2 catalysts at room temperature after treatment *in vacuo* at 773 K.

lectivity in the hydrogenation of ethyl acetate to ethanol (Table 3). As the ratio Sn/Ni increases from 0 to 0.18 the catalytic activity decreases sharply whereas the selectivity to ethanol increases significantly. Above a Sn/Ni ratio of 0.18, both the selectivity to ethanol and the catalytic activity increase with tin content up to a Sn/Ni ratio of 0.36. Above this value, the catalytic activity decreases while the selectivity to ethanol remains constant. With a tin to nickel ratio of 0.36, selectivity to ethanol as high as 96.0% can be obtained for a conversion of ethyl acetate of 2.4%. As shown in Table 3, the selectivity to ethanol decreases very slowly with the conversion; selectivity to ethanol higher than 90% can be observed for conversions of 70%.

The concept of nickel site isolation by tin atoms which may account for the disappearance of bridged CO adsorption on Ni–Sn/SiO_2 catalysts could also explain this high chemoselectivity by a mechanism where the ester group could be coordinated to a single nickel atom with hydrogen transfer to the carbon atom of the carbonyl group followed by a concerted mechanism leading to acetaldehyde (*6*) and nickel alkoxide (which are further hydrogenated to ethanol).

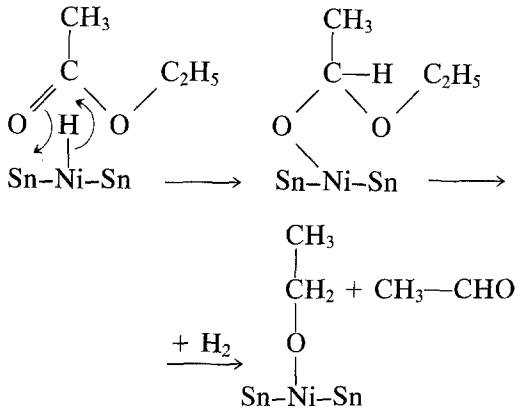

This concept of site isolation is in agreement with the absence of C–C bond cleavage which is known to occur on metallic ensembles (*18*). Nevertheless, this concept could not explain the increase in catalytic activity observed when the Sn/Ni ratio goes from 0.18 to 0.36 (Table 3). An electronic effect of tin on nickel which may account for the CO adsorption infrared band

TABLE 3

Catalytic Activity (r) and Selectivity (S_{EtOH}) of Some Ni–Sn/SiO_2 Catalysts toward Ethyl Acetate Hydrogenolysis for Various Ethyl Acetate Conversions

Sn/Ni	$r \times 10^3$(mol/hg)	X(%)	S_{EtOH}(%)
0	11.1	2.5	53.5
0.18	4.2	1.0	88.0
0.27	7.7	1.7	90.0
0.36	10.5	2.4	96.0
0.51	8.1	1.8	93.6
0.51	—	10.0	93.0
0.51	—	30.0	92.0
0.51	—	70.0	91.0
0.83	4.8	1.1	92.5

Note. T = 523 K; P = 5 MPa; H_2/AcOEt = 9; wwh = 4–40).

shift could explain this enhancement of catalytic activity with tin content.

CONCLUSION

In the course of this work we have been able to demonstrate that the surface reaction between the organostannic compound and nickel oxide occurs above 423 K according to the equation

$$NiO + xSn(n\text{-}C_4H_9)_4 \rightarrow NiSn_x + H_2O + (2x + 1)C_4H_8 + (2x - 1)C_4H_{10}.$$

Various alloy compositions can be obtained by changing the initial Sn/Ni ratio.

Characterization of the bimetallic phase has shown that the particles are bimetallic (STEM), that their average size has increased slightly (from 30 to 40 Å), and that the magnetic property of nickel has been totally cancelled (for a Sn/Ni $\geq$ 0.4). Chemisorption properties of nickel have also been drastically modified in the alloy: H_2 chemisorption uptake has decreased by almost an order of magnitude whereas CO uptake has also been diminished but to a smaller extent. In contrast with nickel which gives linear and bridged chemisorbed CO, the Ni–Sn catalyst gives only a single absorption band corresponding to a linear coordination of CO.

Consequently, the presence of tin has apparently four effects: (i) it significantly decreases the amount of CO and H_2 adsorbed; (ii) it isolates nickel atoms from their neighbors; (iii) it slightly increases the electron density on nickel; (iv) it suppresses the magnetic properties of nickel.

Redox behavior of the Ni – Sn/SiO_2 toward surface OH groups has been also studied. High-temperature evacuation of the reduced Ni–Sn/SiO_2 catalyst results in H_2 evolution due to tin oxidation by surface OH groups. It is suggested that during this oxidation process tin migrates to the periphery of the bimetallic particles with the formation of $(\geqslant Si\text{–}O)_2Sn^{II}$. The process seems to be completely reversible under H_2 at the same temperature (723 K) with regeneration of the bimetallic phase.

The new catalytic phases obtained by the organometallic route exhibit very high selectivity in the hydrogenation of ethyl acetate to ethanol with a maximum in conversion rate obtained for a Sn/Ni ratio equal to 0.36 (Ni_3Sn).

ACKNOWLEDGMENT

M. Agnelli is indebted to the CONICET (Argentina) for financial support.

REFERENCES

1. Ponec, V., *Catal. Rev. Sci. Eng.* **11,** 41 (1975).
2. Sinfelt, J., *J. Catal.* **29,** 308 (1973).
3. Travers, C., Bournonville, J. P., and Martino, G., *in* "Proceeding, 8th International Congress on Catalysis, Berlin, 1984," Vol. IV, p. 891. Dechema, Frankfurt-am-Main, 1984.
4. Ferretti, O. A., Bettega de Paoli, L. C., Candy, J. P., Mabilon, G., and Bournonville J. P., *in* "Preparation of Catalysts. IV. Scientific Bases for the Preparation of Heterogeneous Catalysts" (B. Delmon *et al.*, Eds.), p. 712. Elsevier, Amsterdam/New York, 1987.
5. Candy, J. P., Ferretti O. A., Mabilon, G., Bournonville, J. P., El Mansour, A., Basset, J. M., and Martino, G., *J. Catal.* **112,** 210 (1988).
6. Marcilly, C. H., and Franck, J. P., *Rev. Inst. Fr. Pet.* **39,** 337 (1984).
7. Bartholomew, C. H., and Farrauto, R. J., *J. Catal.* **45,** 41 (1976).
8. Selwood, P. W., *in* "Chemisorption and Magnetization." Academic Press, New York, 1975.
9. Primet, M., Dalmon, J. A., and Martin, G. A., *J. Catal.* **46,** 25 (1977).
10. Bartholomew, C. H., and Pannell, R. B., *J. Catal.* **65,** 390 (1980).
11. Bozorth, R. M., *in* "Ferromagnetism." Van Nostrand, New York, 1951.
12. Margitfalvi, J. L., Göbölös, S., Hegedüs, M., and Talas, E., *in* "Heterogeneous Catalysis and Fine Chemicals" (Guisnet *et al.*, Eds.), p. 145. Elsevier, Amsterdam/New York, 1988.
13. Lieske, H., and Völter, J., *J. Catal.* **90,** 96 (1984).
14. D'Yakonow, Yu., Stytsenko, V. D., Eigenson, I. A., and Rozovskii, Ya., *Kinet. Katal.* **27,** 1398 (1986).
15. Somato-Noto, J., and Sachtler, W. H., *J. Catal.* **32,** 315 (1974).
16. Ichikawa, M., Lang, A. J., Shriver, D. F., and Sachtler W. H., *J. Amer. Chem. Soc.* **107,** 7216 (1985).
17. Galuszka, J., and Amenomiya, J., *in* "Catalysis on the Energy Scene" (S. Kaliaguine and A. Mahay, Eds.), p. 63. Elsevier, Amsterdam/New York, 1984.
18. Dalmon, J. A., and Martin, G. A., *J. Catal.* **66,** 214 (1981).